



Sonothrombolysis Using Microfluidically Produced Microbubbles in a Murine Model of Deep Vein Thrombosis

YanJun Xie¹ · Yi Huang¹ · Hugo C. S. Stevenson¹ · Li Yin^{2,3} · Kaijie Zhang^{2,3} · Zain Husain Islam² · William Aaron Marcum² · Campbell Johnston² · Nicholas Hoyt² · Eric William Kent² · Bowen Wang^{2,3} · John A. Hossack¹

Received: 15 April 2024 / Accepted: 19 August 2024
© The Author(s) 2024

Abstract

The need for safe and effective methods to manage deep vein thrombosis (DVT), given the risks associated with anticoagulants and thrombolytic agents, motivated research into innovative approaches to resolve blood clots. In response to this challenge, sonothrombolysis is being explored as a technique that combines microbubbles, ultrasound, and thrombolytic agents to facilitate the aggressive dissolution of thrombi. Prior studies have indicated that relatively large microbubbles accelerate the dissolution process, either in an *in vitro* or an arterial model. However, sonothrombolysis using large microbubbles must be evaluated in venous thromboembolism diseases, where blood flow velocity is not comparable. In this study, the efficacy of sonothrombolysis was validated in a murine model of pre-existing DVT. During therapy, microfluidically produced microbubbles of 18 μm diameter and recombinant tissue plasminogen activator (rt-PA) were administered through a tail vein catheter for 30 min, while ultrasound was applied to the abdominal region of the mice. Three-dimensional ultrasound scans were performed before and after therapy for quantification. The residual volume of the thrombi was 20% in animals post sonothrombolysis versus 52% without therapy ($p = 0.012 < 0.05$), indicating a significant reduction in DVT volume. Histological analysis of tissue sections confirmed a reduction in DVT volume post-therapy. Therefore, large microbubbles generated from a microfluidic device show promise in ultrasound-assisted therapy to address concerns related to venous thromboembolism.

Keywords Ultrasound · Deep vein thrombosis · Microfluidics · Sonothrombolysis · Microbubble

Introduction

It is estimated that there are more than one million cases involving venous thromboembolism (VTE) annually in the United States. These cases include deep vein thrombosis (DVT) and pulmonary embolism (PE) [1]. DVT not only

contributes to high healthcare expenses [2], but also remains responsible for a one-year mortality rate of 20% [3]. Furthermore, the occurrence of DVT and its sequelae can cause considerable disability and impaired quality of life in individuals after experiencing DVT [4, 5]. Successful treatment of DVT has been shown to be vital in improving long-term outcomes in patients [6, 7].

Standard therapies for acute VTE include oral anticoagulants and reperfusion [8]. With the wide use of oral anticoagulants in clinics, a common side effect is hemorrhage in patients with VTE [9–11]. Meanwhile, systemic infusion of thrombolytic medications, such as recombinant tissue plasminogen activator (rt-PA), results in major bleeding in approximately 3.5% of the patients [12, 13]. It is now more widely accepted that catheter-directed thrombolysis (CDT) delivers smaller doses of thrombolytic agents than systemic infusion for rapid thrombus dissolution [14, 15]. However, the large-scale randomized ATTRACT trial did

Associate Editor Joel Stitzel oversaw the review of this article.

✉ John A. Hossack
jh7fj@virginia.edu

¹ Department of Biomedical Engineering, University of Virginia, 415 Lane Road, Charlottesville, VA 22908, USA

² Department of Surgery, School of Medicine, University of Virginia, 409 Lane Rd MR4, Charlottesville, VA 22908, USA

³ Feinberg School of Medicine, Northwestern University, 300 E. Superior St. Tarry Building, Chicago, IL 60611, USA

not show evidence of improvements in pharmacomechanical CDT (PCDT; CDT with the use of mechanical thrombectomy devices) over oral anticoagulation alone in 2-year post-thrombotic syndrome (PTS) occurrence (47% PCDT vs 48% No-PCDT, $p = 0.56$) [16, 17]. PCDT/CDT should be reserved for highly selected patients with severe symptoms and low bleeding risk. In light of the observations in CDT, there is a need for a safer and more efficient catheterization technique to achieve complete or partial resolution of venous thromboembolism without the risk of hemorrhage.

The use of ultrasound has been demonstrated to enhance the delivery of thrombolytic medications and contrast agents, such as microbubbles (MBs), into blood clots, through acoustic radiation force [18, 19], microstreaming [20, 21], and cavitation [22–24]. In this regard, ultrasound-facilitated thrombolysis, known as sonothrombolysis, has been explored extensively to accelerate blood clot dissolution [25]. The safety profile of such ultrasound-assisted approaches, including intravascular catheter-based ones, has been widely documented [26]. Multiple studies have documented the potential of sonothrombolytic therapies in the *in vitro*, *in vivo*, and *ex vivo* [26–29]. Unfortunately, recent clinical trials have yielded mixed results. While ultrasound-assisted therapies could similarly dissolve DVT, the available evidence did not show significant advantages over CDT therapies [30]. A meta-analysis of clinical trials found that the commercial scheme of Ultrasound-Accelerated Catheter-Directed Thrombolysis (UACDT) without MBs may not be the preferred option due to its prolonged intervention time and marginal improvement in terms of lysis rate [30]. Another clinical study demonstrated that combining therapeutic ultrasound with microbubbles reduced the duration of thrombolysis and allowed for a lower dose of thrombolytic medications [31]. Microbubbles exposed to ultrasound can improve thrombolytic outcomes and should be considered for future therapeutic applications. Studies in animals have also shown potential with the use of microbubbles designed for sonothrombolysis [29, 32, 33]. Collectively, the suboptimal efficacy of existing therapies testifies to the need for further research efforts in improving and refining sonothrombolysis.

Recently, our laboratory has reported sonothrombolysis using large microfluidically produced MBs (>15 μm diameter) [34, 35]. In the *in vivo* study, a 3.3-fold reduction in rt-PA dose was allowed in this stroke model. These studies used a low duty factor (<10%), focusing solely on the mechanical effects of ultrasound, which decreased the thermal effect. Larger microbubbles, compared to commercially available ones, can carry higher momentum under acoustic radiation force [18, 19], and their cavitation can generate more energy [20, 21, 36, 37]. This increase may facilitate the deeper penetration of thrombolytic agents into the thrombus, thereby resulting in improved lysis performance in our

current design than conventional microbubbles. To mitigate the risk of gas embolism, the microbubbles were formed by a nitrogen gas core encapsulated with an albumin shell, which allowed them to dissolve within one minute [35]. Their higher inner pressure compared to the environment also prevented the agglomeration of microbubbles [38, 39].

In this context, there is still an unmet need to validate the efficacy and safety in sonothrombolysis using large MBs through the use of *in vivo* models of DVT, as the mechanical properties and aging of thrombus could vary significantly from prior studies [40, 41]. During thrombosis formation, blood flow velocities differ greatly between veins and arteries. DVT is associated with slow venous flows, whereas arterial thrombosis is often caused by rupture of atherosclerotic plaques [42, 43]. Due to rapid dissolution, sonothrombolysis with these MBs does not produce bio-effects beyond the therapeutic site [35]. Meanwhile, improved efficacy allows DVT therapy with a lower dose of rt-PA than the clinical standard. Therefore, this technique can be used as an adjunctive therapy for patients who might have side effects of hemorrhage in response to thrombolytic agents.

In this work, we investigated the therapeutic efficacy of sonothrombolysis using large microfluidically generated MBs in a mouse model of pre-existing DVT. It was the first *in vivo* study to evaluate the influence of ultrasound and microfluidically produced MBs on venous thromboembolism. For this objective, MBs from a flow-focusing microfluidic device was generated *in situ* and administered to animals through venous catheterization. Microfluidically produced MBs dissolved rapidly in blood flow, thus resulting in limited off-target bioeffects. Changes in blood clot volume were monitored by 3D ultrasound imaging. Based on existing research on CDT in DVT therapy, sonothrombolysis using large microfluidically produced MBs was hypothesized to effectively dissolve the venous thrombus when administered with a reduced dose of rt-PA.

Methods

Fabrication of Microbubbles via Microfluidics

The mold for the microfluidic device was fabricated using the photolithography method, as described in previous research [44, 45]. The device was poured into the SU-8 mold with polydimethylsiloxane (PDMS, Sylgard 184, Dow Corning) and assembled with a clean 500- μm -thick glass wafer. The microfluidic channel had a height of 20 μm and a nozzle width of approximately 7 μm .

MBs were produced using a gas phase of 99.995% N_2 (Linde Gas, Richmond, VA, USA) and a liquid phase of bovine serum albumin (4% w/v), dextrose (10% w/v) in 0.9% saline [45]. The flow rate of the liquid phase was 20

$\mu\text{L}/\text{min}$ supplied by a syringe pump (PhD 2000, Harvard Apparatus, Holliston, MA, USA), and the setting pressure of the gas phase was fixed at 84.8 kPa using a gas regulator (PC-series, Alicat Scientific, Tucson, AZ, USA). The inlets and the outlet of the microfluidic device were connected through 30-gauge inner diameter PTFE tubings (Cole-Parmer, Vernon Hills, IL, USA). The operating parameters were verified to produce MBs in the microfluidic device under a high-speed camera (SIMD24, Specialised Imaging, Tring, UK), optimized as the existing literature [34]. The microbubbles were expected to shrink and quickly dissolve into the environment [39]. Figure S4 illustrates the decrease of microbubble diameter from the production site to the microfluidic device's outlet.

Ultrasound Imaging

All animal experiments followed the guidelines outlined in the Guide for the Care and Use of Laboratory Animals [46] and were conducted in accordance with the approved study protocols by the Animal Care & Use Committee (ACUC) at the University of Virginia (Protocol 4327-09-23). As described in previous literature [47], a high-frequency ultrasound imaging system, Vevo 2100 (FUJIFILM VisualSonics, Toronto, ON, Canada), equipped with a linear array probe MS-550D (40 MHz center frequency) was used to acquire data. The animals were placed on a 37 °C temperature control platform and anesthetized with 1.5% v/v isoflurane. The abdomen of the mice was shaved and treated with ultrasound gel to improve imaging quality. The transducer mounted on a 3D motor module (VisualSonics, Toronto, ON, Canada) captured long-axis slices of mice at a step size of 0.03 mm using B-mode and color Doppler mode. The acquisition was also repeated for the short-axis slice at a step size of 0.1 mm. The mice showing strong color Doppler signals in the IVC were healthy, and they were not enrolled in the study. If color Doppler signals were not continuous or detected in the IVC, another imaging acquisition was performed for additional review. The 3D data collected were saved for further image analysis.

The saved 3D data were exported to 3D Slicer software [48] for annotation and segmentation. After manually labeling multiple 2D slices for a blood clot and background at each view, a grow-from-seeds algorithm was run to semi-automatically segment the blood clot [49]. The volume of the blood clot was then calculated as an output metric. The evaluation of intra- and inter-observer variability is provided in Fig. S2.

Deliverability Study of Microfluidically Produced Microbubbles in Mice

A preliminary investigation was conducted to determine the deliverability of microfluidically produced MBs from a venous catheter to the IVC. Healthy male C57BL/6 mice (8–12 weeks old) were anesthetized with 1.5% isoflurane and placed on a heated 37 °C platform. Microfluidically produced MBs were administered to the tail vein through a catheter for 30 s. B-mode videos were recorded using the ultrasound imaging system described above at 0, 100, and 360 s after administration.

Contrast was used to describe the signal enhancement by the microbubbles. The contrast was defined as [50]

$$C[\text{dB}] = 10 \log_{10} \frac{\mu_v}{\mu_b}, \quad (1)$$

where μ_v , μ_b are the mean signal powers of the regions in the IVC and the background tissue, respectively.

Mouse Model of DVT

A murine IVC partial ligation model was utilized to mimic the venous stenosis/insufficiency and induce the development of DVT, as previously described [51–53]. In total, forty 8-to-12-week old male C57BL/6 mice (The Jackson Laboratory, Bar Harbor, ME, USA) were anesthetized and underwent a midline laparotomy on Day 0. A 30-gauge needle was placed above the IVC as the spacer, and a suture was used to ligate the IVC immediately below the venal vein. The ligation allowed for a 90% closure of the IVC lumen, which resulted in thrombosis without endothelium denudation. After removal of the needle/spacer and wound closure, the mice were recovered and monitored for postoperative care.

The animals were randomly divided into four different therapeutic treatments upon confirmation of DVT development on Day 3 post IVC stenosis, an intermediate time point suggested by [54]. Table 1 summarizes the treatments performed in this study. After 3D ultrasound scanning and reconstruction of the thrombi volume, animals were subjected to the aforementioned therapy session lasting 30 min. Animals in groups A, B, and C were catheterized by an experienced technician and received an

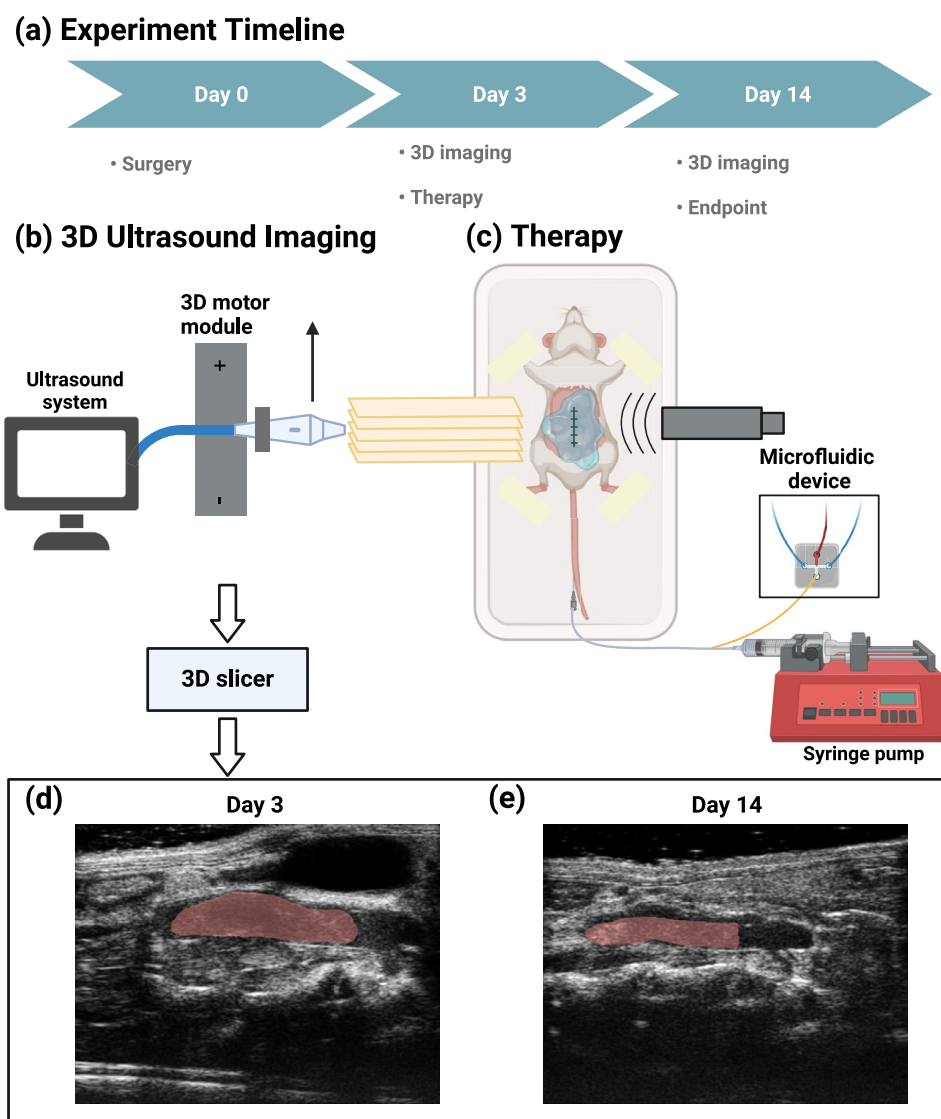
Table 1 Summary of experimental groups

Group	N	rt-PA	Ultrasound	Microbubbles
A	4	+	+	+
B	4	+	+	–
C	4	+	–	–
D	4	–	–	–

injection of 2 mg/kg rt-PA (Activase, Genentech, South San Francisco, CA, USA) [55], while group D was a no-therapy control. The rt-PA dose was administered for a period of 30 min, with an initial bolus of 10%. This dose can lower the risk of major bleeding and was approximately 20% equivalent of a clinical standard dose, since mice have a 10-fold less response to human rt-PA [56, 57]. In groups A and B, a 1-MHz center frequency Panametrics ultrasound transducer (A303S, Olympus Panametrics, Waltham, MA, USA) was placed on the abdomen of mice coupled with ultrasound gel and continuously transmitted energy at a pulse repetition frequency (PRF) of 1 kHz and a duty factor of 2% during the therapy session. The low duty factor allowed for the perfusion of MBs and avoided thermal effects. The transducer was calibrated in a water tank and observed to produce a peak-negative pressure of 574 kPa, at a distance of 7 mm from the

transducer surface. The corresponding intensity I_{spta} was 214 mW/cm², determined by $I_{spta} = P_-^2 / 2\rho c \times DF$, where P_- is the spatial-peak negative pressure, $\rho = 1000 \text{ kg/m}^3$ is the density, $c = 1540 \text{ m/s}$ is the speed of sound and DF is the duty factor of 2% [58]. Since this intensity was below the safety limit of 720 mW/cm², thermal effects were negligible during the therapy using ultrasound [59, 60]. US parameters remained consistent with the calibration. Group A received microfluidically produced MBs for 30 s, every 5 min, as illustrated in Fig. 1. Image sequences of 24 frames were captured using the SIMD24 high-speed camera during the production of microbubbles [45]. In total, 20 MBs were characterized for their outer diameters. The average diameter of the MBs was measured as $18.0 \pm 1.1 \mu\text{m}$ (mean \pm SD), while the production rate was estimated to be 90.3×10^3 MBs per second. Therefore, the total gas volume was approximately 50 μL (Fig. 2).

Fig. 1 **a** Experiment timeline of this study: the animals underwent surgery of partial ligation to develop thrombus on Day 0; 3D ultrasound imaging was performed on Day 3, followed by a therapy; Another 3D ultrasound imaging was conducted on Day 14. **b** Two-dimensional slices of both long axis and short axis view of the IVC were acquired at different vessel cross-sections. Data were exported to 3D Slicer software for segmentation. **c** A therapy to mouse model of DVT. Microfluidically produced MBs and thrombolytic drugs were administered through a tail vein catheter, while ultrasound was applied from the top of the mouse abdomen. Comparison of DVT in the IVC was shown in **d** and **e**, on Days 3 and 14, respectively. The red region indicated the location of thrombus (Color figure online)



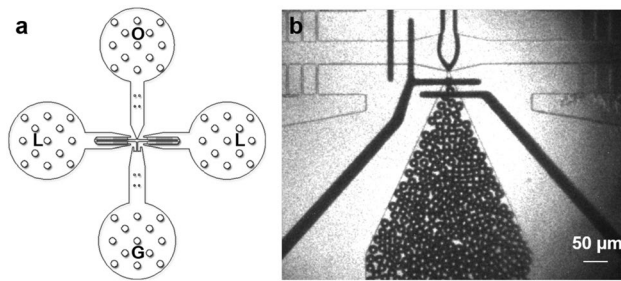


Fig. 2 **a** Layout of a flow-focusing microfluidic device. *G* gas inlet, *L* liquid inlet, *O* MB outlet. **b** A photo of generated MBs under a high speed camera. The mean diameter of MBs was 18.0 μm

On Day 14, a second imaging was performed for the animals under anesthesia, followed by euthanasia. IVC were harvested and preserved in formalin for histological purposes. The residual volume (RV) is defined as:

$$RV(\%) = V_{\text{Day14}}/V_{\text{Day3}} \times 100\%, \quad (2)$$

where V_{Day3} , V_{Day14} are the DVT volume segmented from acquired 3D ultrasound data on Days 3 and 14, respectively. The absolute volume change is calculated by

$$\Delta V = V_{\text{Day14}} - V_{\text{Day3}}. \quad (3)$$

Suggested by a prior study, the resolution of DVT can last for days even with a 10 mg/kg dose of rt-PA [54]. The period of blood clot formation in this study was analogous to that in our research. Therefore, the endpoint of this study was extended to Day 14 to measure noticeable differences in blood clot volume [61, 62].

Histology

Excised IVC specimens were formalin-fixed and paraffin embedded. Sections of 5 μm were obtained at an interval of 0.1 mm across the samples and stained with hematoxylin and eosin (H&E) stain. Slices were scanned with a Leica microscopic camera (DMi8, Leica Microsystems, Durham, NC, USA). Representative photos of each group were selected and demonstrated.

Statistical Analysis

Statistical analysis was performed using RStudio software (R version 4.2.1). Significance in means among all groups was determined using one-way ANOVA, followed by post hoc Fisher's LSD test [63, 64]. The significance level was set at 0.05.

Results

Ultrasound Imaging Assessment of Microfluidically Produced Microbubbles in Mice

Figure 3 shows the B-mode imaging results in mouse IVC. Microfluidically produced MBs injected from a tail vein catheter enhanced the intensity of the B-mode image at 0 s. Due to circulation and gas dissolution, contrast enhancement weakened along with a reduction in the number of detectable MBs 100 s after injection. Eventually, there were no MBs passing through the IVC in 360 s, indicating total absorption of the MBs. The contrast between the vessel and the background tissue regions was 4.5, -7.3, and -6.7 dB at 0, 100, and 360 s, respectively. Most of MBs dissolved into blood flow and did not enhance ultrasound signal intensity at 100 s, as indicated in Fig. 3d. Microfluidically produced MBs can be delivered to the IVC and serve as a thrombolytic agent in sonothrombolysis.

Mouse Model of DVT

Due to the variability inherent to murine models of DVT, not every experimental animal develops thrombosis nor uniformly. In order to focus our studies on animals with pre-existing DVT, a pre-therapy US imaging can screen those mice without DVT. The flowchart of the mice enrolled in this study is presented in Fig. 4. In total, 20 mice were confirmed with DVT by color Doppler ultrasound. Supplementary Fig. S3 displays the mice with DVT or the healthy ones. Only 16 mice with $>5 \text{ mm}^3$ DVT were selected in the experiments. Smaller blood clots can be completely lysed without interventions and the image resolution for them may not be sufficient. All the following data were expressed as mean \pm standard deviation. The mean of initial weight was $28.5 \pm 2.8 \text{ g}$ (A— $29.2 \pm 2.9 \text{ g}$; B— $28.9 \pm 3.3 \text{ g}$; C— $28.5 \pm 2.7 \text{ g}$; D— $27.6 \pm 3.4 \text{ g}$). The mean volume of DVT in all four groups was $15.9 \pm 4.9 \text{ mm}^3$ on Day 3. The initial Day 3 volume in each group was listed below and plotted in Fig. S1: A— $20.0 \pm 6.6 \text{ mm}^3$; B— $16.4 \pm 2.9 \text{ mm}^3$; C— $12.5 \pm 5.1 \text{ mm}^3$; D— $14.8 \pm 2.1 \text{ mm}^3$. The initial volume was not significantly different ($p = 0.18$).

The volume of DVT was evaluated for mice in each experimental group. Representative differences in DVT volume on Days 3 and 14 are shown in Fig. 5, and RVs are plotted in Fig. 6. The average RVs of each group were: (A) microfluidically produced MBs, ultrasound and rt-PA, $20.0 \pm 10.9\%$; (B) ultrasound and rt-PA, $45.3 \pm 18.0\%$; (C) rt-PA, $50.0 \pm 16.1\%$; (D) no-therapy control, $52.2 \pm 15.7\%$. The average absolute loss volume of each group were: (A)

Fig. 3 US images of IVC at **a** 0 s, **b** 100 s, and **c** 360 s after administration of microfluidically produced MBs into the catheter. Cluster of MB flow in the IVC in **a** enhanced the image intensity inside the vein. **b** A single MB traversed in the IVC. **c** No MBs were detected after 360 s. The dash-dotted and dashed rectangles in (**a–c**) indicate the regions of vessel and background tissue, respectively, for contrast calculation. **d** Bar plot for contrast at 0, 100, and 360 s. Error bars show the standard deviation of contrast within the videos

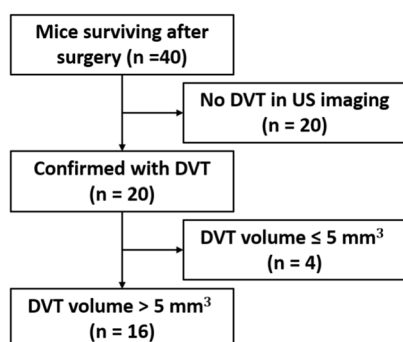
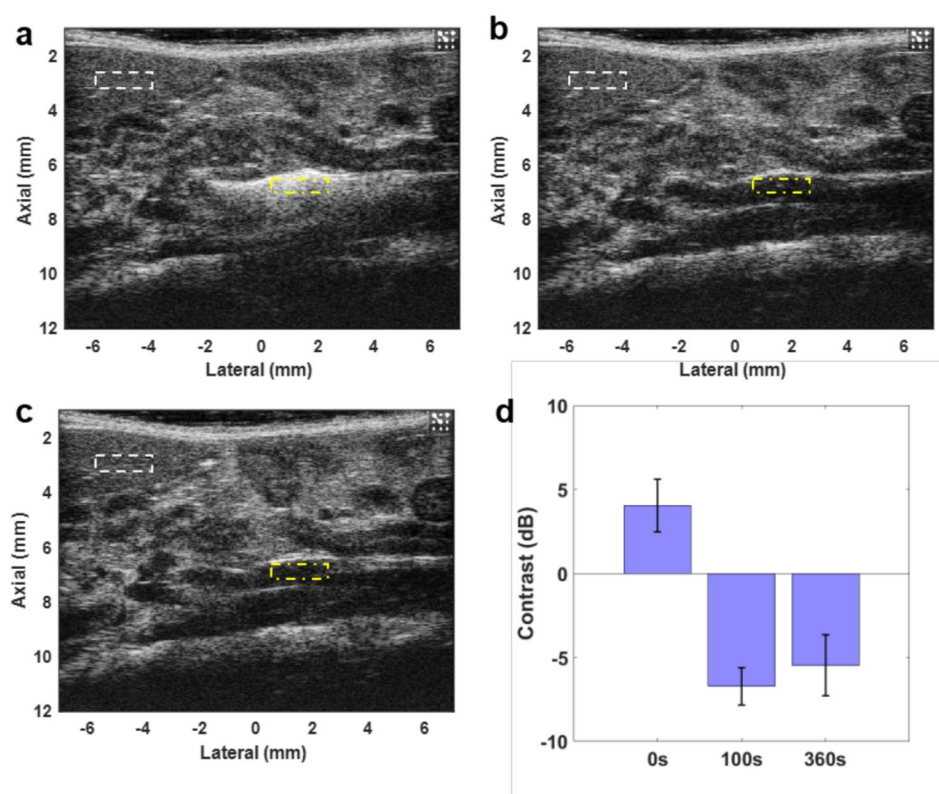


Fig. 4 Flow diagram of mice enrollment in this study

$15.6 \pm 3.7 \text{ mm}^3$; (B) $9.2 \pm 4.0 \text{ mm}^3$; (C) $6.7 \pm 3.9 \text{ mm}^3$; (D) $6.9 \pm 1.8 \text{ mm}^3$.

According to the ANOVA analysis, the average RV for each group was significantly different ($p = 0.0406$). The RV for group A of sonothrombolysis using MBs was significantly different from group B of ultrasound plus rt-PA ($p = 0.0387$), group C of rt-PA alone ($p = 0.0158$), and no-therapy control group D ($p = 0.0121$). Among groups B, C, and D, the RV for group B ultrasound plus rt-PA was not significantly different from group C rt-PA alone ($p = 0.636$) and no-therapy control group D ($p = 0.539$),

neither between group C rt-PA alone and no-therapy control group D ($p = 0.886$).

Similarly, the absolute loss volume showed a significant difference among the four groups ($p = 0.0105$). The absolute reduction volume for group A was significantly different compared to group B ($p = 0.0216$), group C ($p = 0.0032$), and group D ($p = 0.0037$). No significant differences were found among groups B, C, and D.

Histology Results

Representative images of circumferential IVC samples are shown in Fig. 7. The lumen in Fig. 7a was observed with a larger space because the residual blood clot was the smallest among all sections. All residual blood clots in Fig. 7a–d were attached to the IVC vessel walls. The channels within the thrombi were found to allow recanalization, as indicated by the arrows, similar to [65–67], and the fibrin-rich region within the blood clot decreased in group A of sonothrombolysis.

Discussion

This study was the first to evaluate the efficacy of sonothrombolysis using microfluidically produced microbubbles ($>15 \mu\text{m}$) in a murine model of DVT. Microbubbles from a

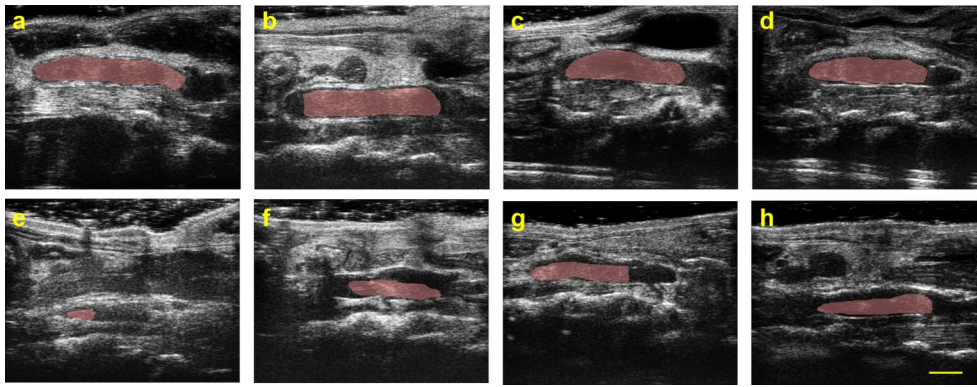


Fig. 5 Representative ultrasound images in long-axis. The top and bottom rows are the results of Day 3 (a–d) and Day 14 (e–h), respectively. Each column is the same mouse from group A sonothrombolysis using microfluidically produced MBs (a, e), B ultrasound plus

rt-PA (b, f), C rt-PA (c, g), and D no-therapy control (d, h). The red overlaid masks are the segmented blood clots. A scalebar of 2 mm is plotted

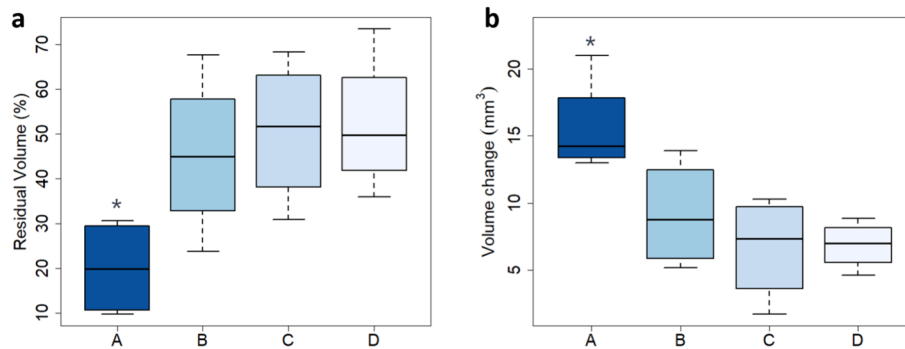


Fig. 6 Efficacy results of therapies. **a** The residual volume of thrombus from Day 3 to Day 14 in percentage is plotted. The use of large microfluidically produced microbubbles reduces the residual volume of thrombus. The differences in the residual volume for MBs + US + rt-PA (group A) and the other groups (B: US + rt-PA; C: rt-PA

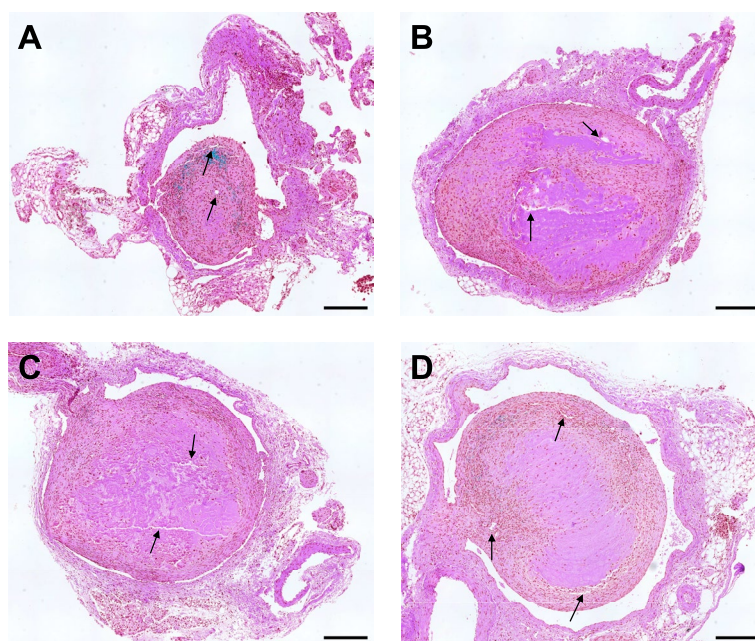
and D: no-therapy control) are all statistically significant ($p < 0.05$, LSD test). **b** Absolute volume change ΔV of each group. An asterisk denotes statistical significance of comparison to no-therapy control group D ($p < 0.05$). Additional statistical results are listed in the result section

microfluidic device were transiently stable, dissolved in the circulation system in minutes (Fig. 3). The use of microbubbles of large diameter in sonothrombolysis applications has previously been proven safe [35]. However, conditions (such as blood flow velocity) in the arteries and veins are not comparable. In addition to differences in arterial and venous thrombus, the age of the thrombus can also affect the therapeutic efficacy of a certain therapy. Catheter-directed intervention for DVT does not show clinical improvement over anticoagulant medications in early-stage DVT, but it is at increased risk of vein injury [17, 68–70]. An appropriate intervention time point for intravenous therapy should be selected for thrombolysis studies. Li et al. propose that patients with intermediate DVT may experience better clinical outcomes when treated with catheter-directed thrombolysis [54]. Therefore, our sonothrombolysis was performed on Day 3 post the surgery. The dissolution of DVT was a gradual process, and the differences in DVT volume required

time to be measured [54]. Our findings of a 14-day timeline can contribute to future research into PTS.

Our mouse model of DVT was created by partial ligation of the IVC, leading to venous stenosis and hemodynamic instability. This model allows for DVT formation while preserving blood flow as observed in clinical DVTs, thereby enabling the delivery of thrombolytic drugs and microbubbles to blood clots. Therefore, it is a suitable animal model for thrombolysis studies. However, this model is associated with a large variance in thrombus size [71]. To mitigate differences in blood clot size, in this study, blood clots less than 5 mm³ were excluded after pre-therapy ultrasound imaging, as in Fig. 4, since smaller clots were generally easier to remove and low risk, even without interventions. In the *in vivo* experiments, the residual volume rate in rt-PA (group C) was not significantly different from the no-therapy control group D, which was consistent with the results of rats with acute carotid artery occlusion [55]. The sub-clinical

Fig. 7 H&E staining results in **a** MBs + US + rt-PA, **b** US + rt-PA, **c** rt-PA, and **d** no-therapy control groups. Arrows in **a–d** show the recanalization channels in thrombus. The scale bar corresponds to 200 μm . *H* & *E* hematoxylin and eosin, *MB* microbubble, *US* ultrasound, *rt-PA* recombinant tissue plasminogen activator



2 mg/kg dose of rt-PA did provide insufficient lysis efficacy. The thrombus volume in the no-therapy control group D decreased by approximately 50% over a period of 14 days, which aligns with the findings of previous studies [72–74]. Furthermore, sonothrombolysis using large microbubbles (group A) displayed significantly improved therapeutic efficacy compared to other control groups in Fig. 6, matching results in the *in vitro* model and the arterial model [34, 35].

The microfluidically produced microbubbles were of 18.0 μm diameter at a production rate of approximately 90×10^3 MBs/s. Large microbubbles have been shown to have stronger bioeffects in applications of blood brain barrier disruption [37], stroke [35], and DVT [27, 34]. A possible explanation for this phenomenon is the increased transfer of momentum induced by acoustic radiation force [18, 19], and higher-energy cavitation events [20, 21]. The administration of microbubbles and thrombolytic agents was performed through a tail vein catheter. Therefore, the routes of intravenous administration should be chosen between a tail vein [35] or femoral veins [75, 76], as they were physically close to the location of the thrombus in the IVC. However, femoral vein injections presented technical difficulties and were not suitable for a study involving long-term survival of mice [77]. Given the number of animals, we use the current scheme to evaluate our performance. Notably, in our experiments, the administration of microbubbles and rt-PA did not result in any mouse fatalities.

Ultrasound applied to cavitate the microbubbles was implemented by an Olympus Panametrics transducer on the abdomen. Catheter-based ultrasound has also been investigated to enable human-compatible dimensions, such as a forward-looking transducer that generates vortex ultrasound

[26, 78, 79], or a side-looking transducer [14, 29, 80, 81]. These therapeutic ultrasound designs can be combined with real-time control of the on-chip microbubbles generation [45]. Advances in the miniaturization of therapeutic ultrasound and microfluidic technology will provide effective therapies for thrombus-related conditions, in the field of catheter-directed therapy. This is an important step toward the miniaturization of human-compatible microfluidic devices for DVT therapy.

The segmentation of the DVT was mostly based on static ultrasound signals. One limitation was due to low sensitivity in the presence of thick adipose tissue. To improve detection of the blood clot boundary, we manually adjusted the imaging plane from the center of abdomen when the imaging quality was affected by shadowing of tissue. The initialization of the algorithm still relied on manual annotation of the thrombus and background [49]. A fully automatic machine learning method can reduce the bias of different experts and generate consistent results among all groups [82]. However, collection and organization of 3D ultrasound dataset of mouse models of DVT might be needed and then used to train or fine-tune a neural network [83]. Representative histological images in Fig. 7 match the quantitative results provided by ultrasound. The smallest cross-sectional area of the residual blood clot is observed in the MBs + US + rt-PA group (A) compared to the other slices. Due to the 50% successful rate of the surgery, the sample size was limited ($N = 4$) and the experiments were conducted in the current conditions. Previous studies have demonstrated the reduction of rt-PA using large microbubbles [34, 35]. Therefore, this research focused on the efficacy of our sonothrombolysis technique in the DVT model. Though the absolute change

in thrombus volume (Fig. 6b) was associated with the initial volume, the initial volume was not significantly different in this study. We chose to use a relative volume metric to represent efficacy.

This study faces certain limitations. First, the stenosis model was used to replicate the reopened thrombus in DVT patients. This model exhibits large variation in thrombus size and fails to mimic a complete occlusion situation. Other models of DVT, such as the stasis model or the electrolytic IVC model, will be used to examine the effectiveness of our sonothrombolysis technique. Secondly, only the symptoms of DVT or bleeding were monitored following the therapy. For clinical translation, it is worth noting that none of the commonly used murine models of DVT - IVC stenosis, IVC stasis (complete ligation), and electric injury - develop PE spontaneously. Recent studies have reported the potential utility of femoral vein stenosis combined with light illumination in recapitulating PE, although further characterization of its robustness and clinical relevance is still warranted [84]. Alternatively, an IVC filter can be implanted to avoid the formation of embolism [85]. In the future, the long-term outcomes using large microbubbles and ultrasound will be investigated. It is essential to assess its efficacy against PTS, which affects patients' quality of life yet still without effective treatments. By leveraging micro-manufacturing techniques, the combination of ultrasound transducers with microfluidic devices will allow for a potential new approach to the resolution of thrombus. In addition to the DVT/PE application considered here, the method has a potential role in the context of cerebral vessels—i.e., stroke. A catheter could be placed within millimeters of the target usage site and generate microbubbles on-site for sonothrombolysis.

Conclusion

At a reduced dose of rt-PA to lessen risk of hemorrhage, large microbubbles were used as a therapeutic agent in a mouse model of DVT, combining with ultrasound and rt-PA. The transiently stable microbubbles produced by a microfluidic device did not cause safety issues in this study, and their use in sonothrombolysis resulted in an improvement in the dissolution of DVT. More research is needed to evaluate the applicability of this technique to other DVT models and its long-term outcomes for PTS. This may involve the development of a human qualified prototype, followed by validation in large animals and then in humans under the appropriate safety controls.

Supplementary Information The online version contains supplementary material available at <https://doi.org/10.1007/s10439-024-03609-7>.

Acknowledgements The authors express gratitude to BioRender for generating a figure. The authors also acknowledge the resources and

services provided by Research Histology Core Facility, a shared facility in the School of Medicine at the University of Virginia. Finally, the authors appreciate Dr. Xinyu Zhou for capturing microscopic images of the sample slides. This research was funded by the National Institute of Health (NIH, R01 HL141752 and HL162895). The opinions expressed in this work are solely the authors' own and do not reflect the official view of the NIH.

Declarations

Conflict of interest All authors declare that they have no Conflict of interest related to this manuscript.

Open Access This article is licensed under a Creative Commons Attribution 4.0 International License, which permits use, sharing, adaptation, distribution and reproduction in any medium or format, as long as you give appropriate credit to the original author(s) and the source, provide a link to the Creative Commons licence, and indicate if changes were made. The images or other third party material in this article are included in the article's Creative Commons licence, unless indicated otherwise in a credit line to the material. If material is not included in the article's Creative Commons licence and your intended use is not permitted by statutory regulation or exceeds the permitted use, you will need to obtain permission directly from the copyright holder. To view a copy of this licence, visit <http://creativecommons.org/licenses/by/4.0/>.

References

1. Tsao, C. W., et al. Heart disease and stroke statistics—2023 update: a report from the American Heart Association. *Circulation*. 147:e93–e621, 2023.
2. Grosse, S. D., R. E. Nelson, K. A. Nyarko, L. C. Richardson, and G. E. Raskob. The economic burden of incident venous thromboembolism in the United States: a review of estimated attributable healthcare costs. *Thrombosis Research*. 137:3, 2016.
3. Minges, K. E., B. Bikkdeli, Y. Wang, R. R. Attaran, and H. M. Krumholz. National and regional trends in deep vein thrombosis hospitalization rates, discharge disposition, and outcomes for medicare beneficiaries. *The American Journal of Medicine*. 131:1200–1208, 2018.
4. Kahn, S. R., et al. Determinants and time course of the Postthrombotic syndrome after acute deep venous thrombosis. *Annals of Internal Medicine*. 149:698–707, 2008.
5. Delis, K. T., D. Bountouroglou, and A. O. Mansfield. Venous claudication in iliofemoral thrombosis. *Annals of Surgery*. 239:118–126, 2004.
6. Avgerinos, E. D., et al. Outcomes and predictors of failure of thrombolysis for iliofemoral deep venous thrombosis. *Journal of Vascular Surgery: Venous and Lymphatic Disorders*. 3:35–41, 2015.
7. Haig, Y., et al. Post-thrombotic syndrome after catheter-directed thrombolysis for deep vein thrombosis (CaVenT): 5-year follow-up results of an open-label, randomised controlled trial. *The Lancet Haematology*. 3:e64–e71, 2016.
8. Becattini, C., and G. Agnelli. Acute treatment of venous thromboembolism. *Blood*. 135:305–316, 2020.
9. Hirsh, J., V. Fuster, J. Ansell, and J. L. Halperin. American Heart Association/American College of Cardiology Foundation Guide to Warfarin Therapy. *Circulation*. 107:1692–1711, 2003.
10. Schulman, S., et al. Extended use of Dabigatran, Warfarin, or Placebo in venous thromboembolism. *New England Journal of Medicine*. 368:709–718, 2013.

11. Weitz, J. I., et al. Rivaroxaban or aspirin for extended treatment of venous thromboembolism. *New England Journal of Medicine*. 376:1211–1222, 2017.
12. Izcovich, A., et al. Thrombolytics for venous thromboembolic events: a systematic review with meta-analysis. *Blood Advances*. 4:1539–1553, 2020.
13. Daley, M. J., M. S. Murthy, and E. J. Peterson. Bleeding risk with systemic thrombolytic therapy for pulmonary embolism: scope of the problem. *Therapeutic Advances in Drug Safety*. 6:57–66, 2015.
14. Dumantepe, M., I. A. Tarhan, and A. Ozler. Treatment of chronic deep vein thrombosis using ultrasound accelerated catheter-directed thrombolysis. *European Journal of Vascular and Endovascular Surgery*. 46:366–371, 2013.
15. Goldhaber, S. Z., E. A. Magnuson, K. M. Chinnakondepalli, D. J. Cohen, and S. Vedantham. Catheter-directed thrombolysis for deep vein thrombosis: 2021 update. *Vascular Medicine*. 26:662–669, 2021.
16. Vedantham, S., et al. Pharmacomechanical catheter-directed thrombolysis for deep-vein thrombosis. *New England Journal of Medicine*. 377:2240–2252, 2017.
17. Winokur, R. S., and A. K. Sista. DVT intervention in the post-ATT RACT era. *Current Treatment Options in Cardiovascular Medicine*. 20:70, 2018.
18. Dayton, P. A., J. S. Allen, and K. W. Ferrara. The magnitude of radiation force on ultrasound contrast agents. *The Journal of the Acoustical Society of America*. 112:2183–2192, 2002.
19. Chuang, Y., P. Cheng, and P. Li. Combining radiation force with cavitation for enhanced sonothrombolysis. *IEEE Transactions on Ultrasonics, Ferroelectrics, and Frequency Control*. 60:97–104, 2013.
20. Marmottant, P., and S. Hilgenfeldt. Controlled vesicle deformation and lysis by single oscillating bubbles. *Nature*. 423:153–156, 2003.
21. Wu, J. Theoretical study on shear stress generated by microstreaming surrounding contrast agents attached to living cells. *Ultrasound in Medicine & Biology*. 28:125–129, 2002.
22. Prentice, P., A. Cuschieri, K. Dholakia, M. Prausnitz, and P. Campbell. Membrane disruption by optically controlled microbubble cavitation. *Nature Physics*. 1:107–110, 2005.
23. Ohl, C.-D., et al. Sonoporation from jetting cavitation bubbles. *Biophysical Journal*. 91:4285–4295, 2006.
24. Chen, H., W. Kreider, A. A. Brayman, M. R. Bailey, and T. J. Matula. Blood vessel deformations on microsecond time scales by ultrasonic cavitation. *Physical Review Letters*. 106:034301, 2011.
25. Bader, K. B., Bouchoux, G. & Holland, C. K. in *Sonothrombolysis* (eds Escoffre, J.-M. & Bouakaz, A.) *Therapeutic Ultrasound*, Vol. 880 339–362 (Springer International Publishing, Cham, 2016).
26. Goel, L., et al. Safety evaluation of a forward-viewing intravascular transducer for sonothrombolysis: an in vitro and ex vivo study. *Ultrasound in Medicine & Biology*. 47:3231–3239, 2021.
27. Borrelli, M. J., et al. Influences of microbubble diameter and ultrasonic parameters on in vitro sonothrombolysis efficacy. *Journal of Vascular and Interventional Radiology*. 23:1677–1684.e1, 2012.
28. Engelberger, R. P., et al. Enhanced thrombolysis by ultrasound-assisted catheter-directed thrombolysis and microbubbles in an in vitro model of iliofemoral deep vein thrombosis. *Thrombosis and Haemostasis*. 119:1094–1101, 2019.
29. Wang, Z., et al. Enhanced thrombolysis by endovascular low-frequency ultrasound with bifunctional microbubbles in venous thrombosis: in vitro and in vivo study. *Frontiers in Bioengineering and Biotechnology*. 2022. <https://doi.org/10.3389/fbioe.2022.965769>.
30. Shi, Y., W. Shi, L. Chen, and J. Gu. A systematic review of ultrasound-accelerated catheter-directed thrombolysis in the treatment of deep vein thrombosis. *Journal of Thrombosis and Thrombolysis*. 45:440–451, 2018.
31. Zhu, Q., et al. Intra-clot microbubble-enhanced ultrasound accelerates catheter-directed thrombolysis for deep vein thrombosis: a clinical study. *Ultrasound in Medicine & Biology*. 45:2427–2433, 2019.
32. Wang, S., et al. Accelerating thrombolysis using a precision and clot-penetrating drug delivery strategy by nanoparticle-shelled microbubbles. *Science Advances*. 2020. <https://doi.org/10.1126/sciadv.aaz8204>.
33. Chen, J., et al. Targeted microbubbles combined with low-power focused ultrasound promote the thrombolysis of acute deep vein thrombosis. *Frontiers in Bioengineering and Biotechnology*. 11:1163405, 2023.
34. Dixon, A. J., J. M. R. Rickel, B. D. Shin, A. L. Klibanov, and J. A. Hossack. In vitro sonothrombolysis enhancement by transiently stable microbubbles produced by a flow-focusing microfluidic device. *Annals of Biomedical Engineering*. 46:222–232, 2018.
35. Dixon, A. J., et al. Efficacy of sonothrombolysis using microbubbles produced by a catheter-based microfluidic device in a rat model of ischemic stroke. *Annals of Biomedical Engineering*. 47:1012–1022, 2019.
36. van Elburg, B., et al. Dependence of sonoporation efficiency on microbubble size: an in vitro monodisperse microbubble study. *Journal of Controlled Release*. 363:747–755, 2023.
37. Choi, J., et al. Microbubble-size dependence of focused ultrasound-induced blood-brain barrier opening in mice in vivo. *IEEE Transactions on Biomedical Engineering*. 57:145–154, 2010.
38. Dhanaliwala, A. H., et al. In vivo imaging of microfluidic-produced microbubbles. *Biomed Microdevices*. 2015. <https://doi.org/10.1007/s10544-014-9914-9>.
39. Kabalnov, A., D. Klein, T. Pelura, E. Schutt, and J. Weers. Dissolution of multicomponent microbubbles in the bloodstream: I theory. *Ultrasound in Medicine & Biology*. 24:739–749, 1998.
40. Chernysh, I. N., et al. The distinctive structure and composition of arterial and venous thrombi and pulmonary emboli. *Scientific Reports*. 10:5112, 2020.
41. Stocker, G. E., et al. In vivo porcine aged deep vein thrombosis model for testing ultrasound-based thrombolysis techniques. *Ultrasound in Medicine & Biology*. 47:3447–3457, 2021.
42. Stone, J., et al. Deep vein thrombosis: pathogenesis, diagnosis, and medical management. *Cardiovascular Diagnosis and Therapy*. 7:S276–S284, 2017.
43. Koupounova, M., B. E. Kehrel, H. A. Corkrey, and J. E. Freedman. Thrombosis and platelets: an update. *European Heart Journal*. 38:785–791, 2017.
44. Dhanaliwala, A. H., J. L. Chen, S. Wang, and J. A. Hossack. Liquid flooded flow-focusing microfluidic device for in situ generation of monodisperse microbubbles. *Microfluid Nanofluid*. 14(3–4):457–467, 2013.
45. Xie, Y., A. J. Dixon, J. M. R. Rickel, A. L. Klibanov, and J. A. Hossack. Closed-loop feedback control of microbubble diameter from a flow-focusing microfluidic device. *Biomed Microfluidics*. 14:034101, 2020.
46. National Research Council (US) Institute for Laboratory Animal Research. *Guide for the Care and Use of Laboratory Animals* (National Academies Press (US), Washington (DC), 1996).
47. Xie, Y., et al. A quantitative method for the evaluation of deep vein thrombosis in a murine model using three-dimensional ultrasound imaging. *Biomedicine*. 12:200, 2024.
48. Kikinis, R., Pieper, S. D. & Vosburgh, K. G. in *3D Slicer: A Platform for Subject-Specific Image Analysis, Visualization, and Clinical Support* (ed. Jolesz, F. A.) *Intraoperative Imaging and Image-Guided Therapy* 277–289 (Springer, New York, NY, 2014).

49. Zhu, L., Kolesov, I., Gao, Y., Kikinis, R. & Tannenbaum, A. "" (ed.) *An effective interactive medical image segmentation method using fast growcut*. (ed."") *MICCAI Workshop on Interactive Medical Image Computing* (2014)
50. Rodriguez-Molares, A., et al. The generalized contrast-to-noise ratio: a formal definition for lesion detectability. *IEEE Transactions on Ultrasonics, Ferroelectrics, and Frequency Control*. 67:745–759, 2020.
51. Brill, A., et al. Von Willebrand factor-mediated platelet adhesion is critical for deep vein thrombosis in mouse models. *Blood*. 117:1400–1407, 2011.
52. Geddings, J., et al. Strengths and weaknesses of a new mouse model of thrombosis induced by inferior vena cava stenosis: communication from the SSC of the ISTH. *Journal of Thrombosis and Haemostasis*. 12:571–573, 2014.
53. von Brühl, M.-L., et al. Monocytes, neutrophils, and platelets cooperate to initiate and propagate venous thrombosis in mice in vivo. *The Journal of Experimental Medicine*. 209:819–835, 2012.
54. Li, W., et al. Time-restricted salutary effects of blood flow restoration on venous thrombosis and vein wall injury in mouse and human subjects. *Circulation*. 143:1224–1238, 2021.
55. Tomkins, A. J., R. J. Hood, C. R. Levi, and N. J. Spratt. Tissue plasminogen activator for preclinical stroke research: neither “rat” nor “human” dose mimics clinical recanalization in a carotid occlusion model. *Scientific Reports*. 5:16026, 2015.
56. Kucher, N., et al. Randomized, controlled trial of ultrasound-assisted catheter-directed thrombolysis for acute intermediate-risk pulmonary embolism. *Circulation*. 129:479–486, 2014.
57. Korninger, C., and D. Collen. Studies on the specific fibrinolytic effect of human extrinsic (tissue-type) plasminogen activator in human blood and in various animal species in vitro. *Thrombosis and Haemostasis*. 46:561–565, 1981.
58. Sun, Y., D. E. Kruse, and K. W. Ferrara. Contrast imaging with chirped excitation. *IEEE Transactions on Ultrasonics, Ferroelectrics, and Frequency Control*. 54:520–529, 2007.
59. Health, C. f. D. a. R. Marketing clearance of diagnostic ultrasound systems and transducers. <https://www.fda.gov/regulatory-information/search-fda-guidance-documents/marketing-clearance-diagnostic-ultrasound-systems-and-transducers>. Accessed 13 Feb 2023
60. ter Haar, G. Ultrasonic imaging: safety considerations. *Interface Focus*. 1:686–697, 2011.
61. Cooley, B. C., and G. Schmeling. Murine model of large-vein electrolytic injury induction of thrombosis with slow resolution. *Thrombosis Research*. 140:149–152, 2016.
62. Singh, S., A. K. Houg, and G. L. Reed. Venous stasis-induced fibrinolysis prevents thrombosis in mice: role of $\alpha 2$ -antiplasmin. *Blood*. 134:970–978, 2019.
63. Silveira, P. C. L., et al. Effects of therapeutic pulsed ultrasound and dimethylsulfoxide (DMSO) phonophoresis on parameters of oxidative stress in traumatized muscle. *Ultrasound in Medicine & Biology*. 36:44–50, 2010.
64. Huber, P. E., and P. Pfisterer. In vitro and in vivo transfection of plasmid DNA in the dunning prostate tumor R3327-AT1 is enhanced by focused ultrasound. *Gene Therapy*. 7:1516–1525, 2000.
65. Comerota, A. J., et al. A histological and functional description of the tissue causing chronic postthrombotic venous obstruction. *Thrombosis Research*. 135:882–887, 2015.
66. Dickhout, A., et al. Molecular detection of venous thrombosis in mouse models using SPECT/CT. *Biomolecules*. 12:829, 2022.
67. Shi, W.-Y., S. Wu, L.-Y. Hu, C.-J. Liu, and J.-P. Gu. Swine model of thrombotic caval occlusion created by autologous thrombus injection with assistance of intra-caval net knitting. *Scientific Reports*. 5:18546, 2015.
68. Weitz, J. I., and N. C. Chan. Novel antithrombotic strategies for treatment of venous thromboembolism. *Blood*. 135:351–359, 2020.
69. Kessinger, C. W., et al. Statins improve the resolution of established murine venous thrombosis: reductions in thrombus burden and vein wall scarring. *PLoS ONE*. 10:e0116621, 2015.
70. Nathan, A. S., and J. Giri. Reexamining the open-vein hypothesis for acute deep venous thrombosis. *Circulation*. 139:1174–1176, 2019.
71. Diaz, J. A., et al. Choosing a mouse model of venous thrombosis. *Arteriosclerosis, Thrombosis, and Vascular Biology*. 39:311–318, 2019.
72. Zhao, L., et al. Measurement of thrombus resolution using three-dimensional ultrasound assessment of deep vein thrombosis volume. *Journal of Vascular Surgery: Venous and Lymphatic Disorders*. 2:140–147, 2014.
73. Singh, I., et al. Failure of thrombus to resolve in urokinase-type plasminogen activator gene-knockout mice. *Circulation*. 107:869–875, 2003.
74. Humphries, J., et al. Monocyte urokinase-type plasminogen activator up-regulation reduces thrombus size in a model of venous thrombosis. *Journal of Vascular Surgery*. 50:1127–1134, 2009.
75. Alonso, A., et al. In vivo clot lysis of human thrombus with intravenous abciximab immunobubbles and ultrasound. *Thrombosis Research*. 124:70–74, 2009.
76. Wang, X., et al. Novel single-chain antibody-targeted microbubbles for molecular ultrasound imaging of thrombosis. *Circulation*. 125:3117–3126, 2012.
77. Prathipati, P., et al. A retrospective analysis for different routes of administration in mice-percutaneous retro-orbital, jugular catheter, tail vein and femoral cut down injections. *Journal of Biosciences and Medicines*. 08:131, 2020.
78. Zhang, B., et al. A model of high-speed endovascular sonothrombolysis with vortex ultrasound-induced shear stress to treat cerebral venous sinus thrombosis. *Research*. 6:0048, 2023.
79. Kim, H., et al. Vortex-ultrasound for microbubble-mediated thrombolysis of retracted clots. *Applied Physics Letters*. 123:073701, 2023.
80. Li, P., W. Huang, J. Xu, W. Shao, and Y. Cui. Efficacy estimation of microbubble-assisted local sonothrombolysis using a catheter with a series of miniature transducers. *Micromachines*. 12:612, 2021.
81. Kuliha, M., et al. Safety and efficacy of endovascular sonolysis using the Ekosonic endovascular system in patients with acute stroke. *American Journal of Neuroradiology*. 34:1401–1406, 2013.
82. Kainz, B., et al. Non-invasive diagnosis of deep vein thrombosis from ultrasound imaging with machine learning. *NPJ Digital Medicine*. 4:1–18, 2021.
83. Amiri, M., R. Brooks, and H. Rivaz. Fine-tuning U-NET for ultrasound image segmentation: different layers, different outcomes. *IEEE Transactions on Ultrasonics, Ferroelectrics, and Frequency Control*. 67:2510–2518, 2020.
84. Okano, M., et al. In vivo imaging of venous thrombus and pulmonary embolism using novel murine venous thromboembolism model. *JACC: Basic to Translational Science*. 5:344–356, 2020.
85. Sharifi, M., C. Bay, L. Skrocki, D. Lawson, and S. Mazdeh. Role of IVC filters in endovenous therapy for deep venous thrombosis: the filter-PEVI (filter implantation to lower thromboembolic risk in percutaneous endovenous intervention) trial. *Cardio Vascular and Interventional Radiology*. 35:1408–1413, 2012.

Publisher's Note Springer Nature remains neutral with regard to jurisdictional claims in published maps and institutional affiliations.